# XXI. PLASMAS AND CONTROLLED NUCLEAR FUSION

## A. Active Plasma Systems*

### Academic and Research Staff

Prof. L. D. Smullin, Prof. G. D. Bernard, Prof. R. J. Briggs, Prof. A. Bers, Prof. J. G. Siambis

### Graduate Students

R. R. Bartsch, F. N. Herba, D. M. Perozek, S. R. J. Brueck, B. R. Kusse, H. M. Schneider, S-L. Chou, O. Lopez, R. E. Tremain, Jr., J. A Davis, J. A. Mangano, R. N. Wallace, R. R. Parker

### RESEARCH OBJECTIVES

1. Beam-Plasma Discharge

Our principal research effort will go into the study of means of transferring the greatest amount of power from a beam to its resultant plasma. Experimentally, this will involve the redesign of System D in such a way as to permit easier variation of gun parameters, and beam powers up to 1 MW, or so, will be used. Also, the redesign will provide greater pumping speed and will allow the use of highly conducting end plates just outside the mirrors to provide "magnetic line-tieing."

Other studies will continue the work on excitation of ion motion by modulating the beam at an appropriate frequency between the ion-cyclotron and the hybrid frequency.

2. Beam-Plasma Interactions: Experiments and Theory

During the past year, we have observed beam-plasma interactions that lead to self-excited ion oscillations in the vicinity of the ion plasma frequency $\omega_{pi}$. Our effort now is to establish an appropriate theoretical model that will explain these observations and ellucidate the role of hot electrons.

A velocity analysis of the emerging beam in System A has been obtained. Theoretical work on the nonlinear aspects of beam-plasma interactions is being carried out in order to obtain a quantitative picture of the energy loss by the beam.

Experiments have been initiated to study the nature of beam-plasma interactions when the injected beam has a considerable fraction of its energy across the applied magnetic field. Low-frequency oscillations and a diocotron-type breakup of the beam have been observed.

3.. Active Plasma Effects in Solids

We plan to continue our theoretical studies of plasma instabilities in solids that may be of interest for high-frequency generation and amplification. An analysis of acoustic-wave growth in the presence of electron drift along an applied magnetic field has been completed. The analysis of quantum effects that become important at high frequencies continues. Other modes under study are the drifted-helicon wave with its self-magnetic field, and nonlocal effects on the helicon surface-wave mode.

L. D. Smullin, A. Bers, R. J. Briggs, R. R. Parker

*This work was supported by the National Science Foundation (Grants GK-57 and GK-1165)

## 1. SYSTEM C: ION-CYCLOTRON WAVE GENERATION

The study of ion-cyclotron wave excitation and propagation in System C has been completed and the results will be submitted to the Department of Electrical Engineering, M. I. T., as an Sc. D. thesis.

One of the results of this study is the solution of the eigenvalue problem previously posed.[1] In addition to the exact solution, we have obtained good approximate solutions in two mutually exclusive regions of plasma parameters, one of which corresponds to the "zero-electron mass" approximation.

R. R. Parker

### References

1. R. R. Parker, Quarterly Progress Report No. 82, Research Laboratory of Electronics, M. I. T., July 15, 1966, pp. 127-131.

## 2. BEAM-PLASMA DISCHARGE: SYSTEM D

### Oscillations Stimulated by a DC Beam

A DC beam has been injected into the afterglow of the beam-plasma discharge to study the interaction of a low-energy (<1 kV) beam with a plasma that has a significant fraction of its electron density in the form of hot electrons. We see oscillations in the 250-1000 Mc range, which cease at the times corresponding to the electron plasma frequency (as determined by the previously measured density decay), dropping below the particular frequency that is being observed. Low-frequency oscillations in the range 1-50 Mc are observed 50-150 msec after the main discharge. We are now attempting to correlate these observations with the work of Lieberman.[1]

### Characteristics of the Unstable Afterglow

The DC beam described above triggers an instability when the gas pressure is below the level of normal operation. One characteristic of this instability is a sharp drop in the diamagnetism. Since we can interpret rapid (<5-10 msec) changes in the diamagnetism, we can use this instability to determine the plasma diamagnetism at times in the afterglow that are greater than the flux diffusion time through the discharge-tube wall. The range of observed diamagnetism is shown in Fig. XXI-1, wherein we have assumed that all of the hot electrons are lost in the instability, that is, the diamagnetism of the plasma drops to zero.

Previously reported observations[2] of oscillations following the occurrence of an instability have been extended. The oscillations are observed as low as 1 kMc – lower than the electron cyclotron frequency (~3 kMc). Raising the magnetic field ~50 per cent

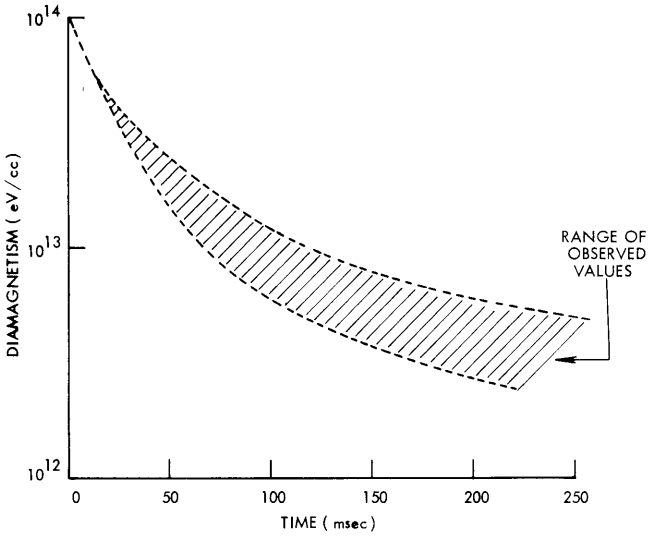


Fig. XXI-1. Plasma diamagnetism determined from triggered instability.

does not eliminate the oscillations near 1 kMc.

The particle flux to the walls and ends of the system following an instability has been observed. The net current out of the ends of the system is negative, and the net current to the walls is positive. If this is interpreted as meaning that electrons are lost axially and ions radially, the currents approximately account for the total number of particles in the system at the time of the instability.

## Pressure Measurements

The Veeco-Gauge gauge factor has been determined with a McLeod gauge to be two for hydrogen, in agreement with data furnished by Veeco.[3] The pressure transient for the Marshall valve is shown in Fig. XXI-2. The upper curve is the pressure ~2 inches in front of the collector, and the lower curve is the pressure at the gun end of the system. The peak pressure was adjusted to be the same as the peak pressure used for previously reported measurements of the discharge characteristics.

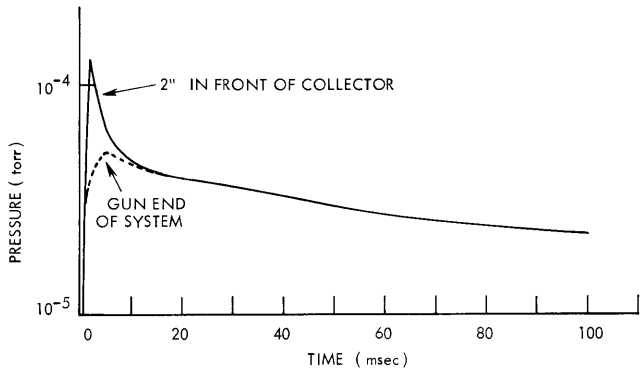


Fig. XXI-2. Marshall valve pressure transient.

X-ray spectrum measurements are now being made to determine the temperature of the hot electrons. A

beryllium window and a thin sodium iodide scintillation crystal are being installed to facilitate measurement of the spectrum down to 10 keV.

The author wishes to acknowledge the use of the facilities of the National Magnet Laboratory for the experiments described above.

R. R. Bartsch

References

1. M. A. Lieberman, Ph. D. Thesis, Department of Electrical Engineering, M. I. T., June 1966.
2. R. R. Bartsch, Quarterly Progress Report No. 83, Research Laboratory of Electronics, M. I. T., October 15, 1966, pp. 65-72.
3. P. Becker, Veeco Instruments, Inc. (Private communication, 1966).

## 3. CROSS-FIELD BEAM-PLASMA EXPERIMENT

Preliminary experiments have been carried out on the cross-field beam-plasma apparatus described in a previous report.[1] In these initial observations three types of beams have been used: (i) an axially flowing hollow beam obtained by having $B_r$ and $B_L$, as previously described,[1] pointing in the same direction and equal in magnitude; (ii) an axially flowing hollow beam rotating about its axis obtained by having $B_L$ and $B_r$ oppositely directed and equal in magnitude; and (iii) an axially flowing scalloped beam obtained by setting $B_L = 0$.

With any of these beams it is possible to operate the discharge in two regimes. The first regime is characterized by ionization of the gas only in the region of the beam. The second regime is encountered by increasing the pressure of the background gas and the perveance of the beam. In the last regime a beam-plasma discharge takes place, and gas in the entire drift region can be ionized.

The initial measurements have shown low-frequency, narrow-bandwidth oscillations to be present in the low pressure-low perveance regime. These oscillations range in frequency from 10 to 200 kHz, and in some cases are essentially pure sine waves. Oscillations also have been observed in the beam-plasma-discharge regime. These oscillations are of wider bandwidth and higher in frequency (~100 mHz) than the low-frequency oscillations.

Experiments are now being carried out to verify a thin-beam electrostatic model of the system operating in the low pressure-low perveance regime.

B. R. Kusse, A. Bers

References

1. B. Kusse and A. Bers, "Cross-Field Beam-Plasma Interactions," Quarterly Progress Report No. 82, Research Laboratory of Electronics, M. I. T., July 15, 1966, pp. 154-157.

## 4. SHEET MODELS OF THE BEAM-PLASMA DISCHARGE WITH PLASMA DENSITY GRADIENTS ALONG THE BEAM

Previously, we found we had to include a very large collision frequency ($\nu = 0.2\omega_p$) to justify our assumption that the plasma remained linear at the point of initial beam overtaking.[1] In this case the plasma had a uniform density, and we velocity-modulated the beam at the plasma frequency. We find that the introduction of a longitudinal plasma density gradient produces a much less intense interaction, even in the absence of collisions or temperature. If we velocity-modulate the beam at the local plasma frequency near the gun, this frequency will be different from the local plasma frequency at the point of initial overtaking. That is, the bunches formed at overtaking will strike the plasma off-resonance, and the fields there will be much less.

### Linear Theory: Continuum Model

We shall now derive the linearized equations for a beam-plasma interaction with the plasma density increasing linearly from the gun. We shall then compare computer experiments with these linearized results.

The model is one-dimensional, with a cold, collisionless plasma whose density is given by

$$\omega_p^2(z) = \omega^2 + a\,z. \tag{1}$$

We assume that all variables oscillate at $\omega$, the local plasma frequency at $z = 0$.

$$i\,m\,\omega\,v_p = e\,E$$

$$i\,m\,\omega\,v_b + m\,v_{ob}\frac{\partial v_b}{\partial z} = e\,E \tag{3}$$

$$\frac{\partial E}{\partial z} = \frac{\rho_p + \rho_b}{\epsilon_o} \tag{4}$$

$$\frac{\partial}{\partial z}\left[\rho_{op}(z)\,v_p\right] = -i\,\omega\,\rho_p \tag{5}$$

$$\frac{\partial}{\partial z}\left[\rho_{ob}\,v_b + \rho_b\,v_o\right] = -i\,\omega\,\rho_b, \tag{6}$$

where $v_p$, $\rho_p$, $v_b$, $\rho_b$ are the first-order velocities and charge densities, and $\rho_{ob}$ is assumed constant. By manipulation of Eqs. 1-6, we obtain

$$v_o\,a\,z\frac{\partial^2 v_b}{\partial z^2} + \left[a\,v_o + i\,2\omega\,a\,z\right]\frac{\partial v_b}{\partial z} + \left[i\,\omega\,a - \frac{\omega^2}{v_o}\left(a\,z + \omega_{pb}^2\right)\right]v_b = 0. \tag{7}$$

The solutions to Eq. 6, for $z < 0$, are

$$v_{bI} \sim \exp\left(\frac{-i\omega z}{v_o}\right) J_o\left[\frac{2\omega\omega_{pb}}{v_o}\left(\frac{-z}{a}\right)^{1/2}\right] \tag{8}$$

$$v_{bII} \sim \exp\left(\frac{-i\omega z}{v_o}\right) Y_o\left[\frac{2\omega\omega_{pb}}{v_o}\left(\frac{-z}{a}\right)^{1/2}\right], \tag{9}$$

and for $z > 0$,

$$v_{bI} \sim \exp\left(\frac{-i\omega z}{v_o}\right) I_o\left[\frac{2\omega\omega_{pb}}{v_o}\left(\frac{z}{a}\right)^{1/2}\right] \tag{10}$$

$$v_{bII} \sim \exp\left(\frac{-i\omega z}{v_o}\right) K_o\left[\frac{2\omega\omega_{pb}}{v_o}\left(\frac{z}{a}\right)^{1/2}\right]. \tag{11}$$

The expressions for the other variables can be obtained from Eqs. 1-6. In particular,

$$E_I = v_{bI}\frac{m}{e}\frac{\omega\omega_{pb}}{v_o\sqrt{az}}\exp\left(\frac{-i\omega z}{v_o}\right) I_1\left[\frac{2\omega\omega_{pb}}{v_o}\left(\frac{z}{a}\right)^{1/2}\right]; \quad z > 0 \tag{12}$$

The physical meanings of the $v_{bII}$ solutions are still unclear. Attempts to excite them in computer experiments have failed, thus far. We note that if "a" were negative (a linearly decreasing density) the solutions for $z > 0$ and $z < 0$ would be reversed.

## Nonlinear Theory: Computer Sheet Model

For "a" positive, the $I_o$ solution is easily excited in a computer experiment. This calculation was done as reported previously,[1] except a Runge-Kutta integration technique was used throughout, in place of the Milne method. Energy conservation is now better than 0.5 per cent. Snapshots of normalized beam-sheet velocity and acceleration (-eE/m) versus distance are shown in Figs. XXI-3 and XXI-4. The solid lines in each figure indicate the predictions of the linear theory. Times are normalized to $\omega_{po}$, distances to $0.4\,v_o/\omega_{po}$. The density is $\rho_o(z) = 0.15\,\rho_o + 0.001\,z$.

The plasma first-order charge density is approximately 11 per cent of $\rho_o(z)$ at the point of maximum field. With a suitable correction for finite beam diameter, it should be even less. This matter is under study at present.

J. A. Davis

## References

1. J. A. Davis, Quarterly Progress Report No. 81, Research Laboratory of Electronics, M.I.T., April 15, 1966, p. 146.

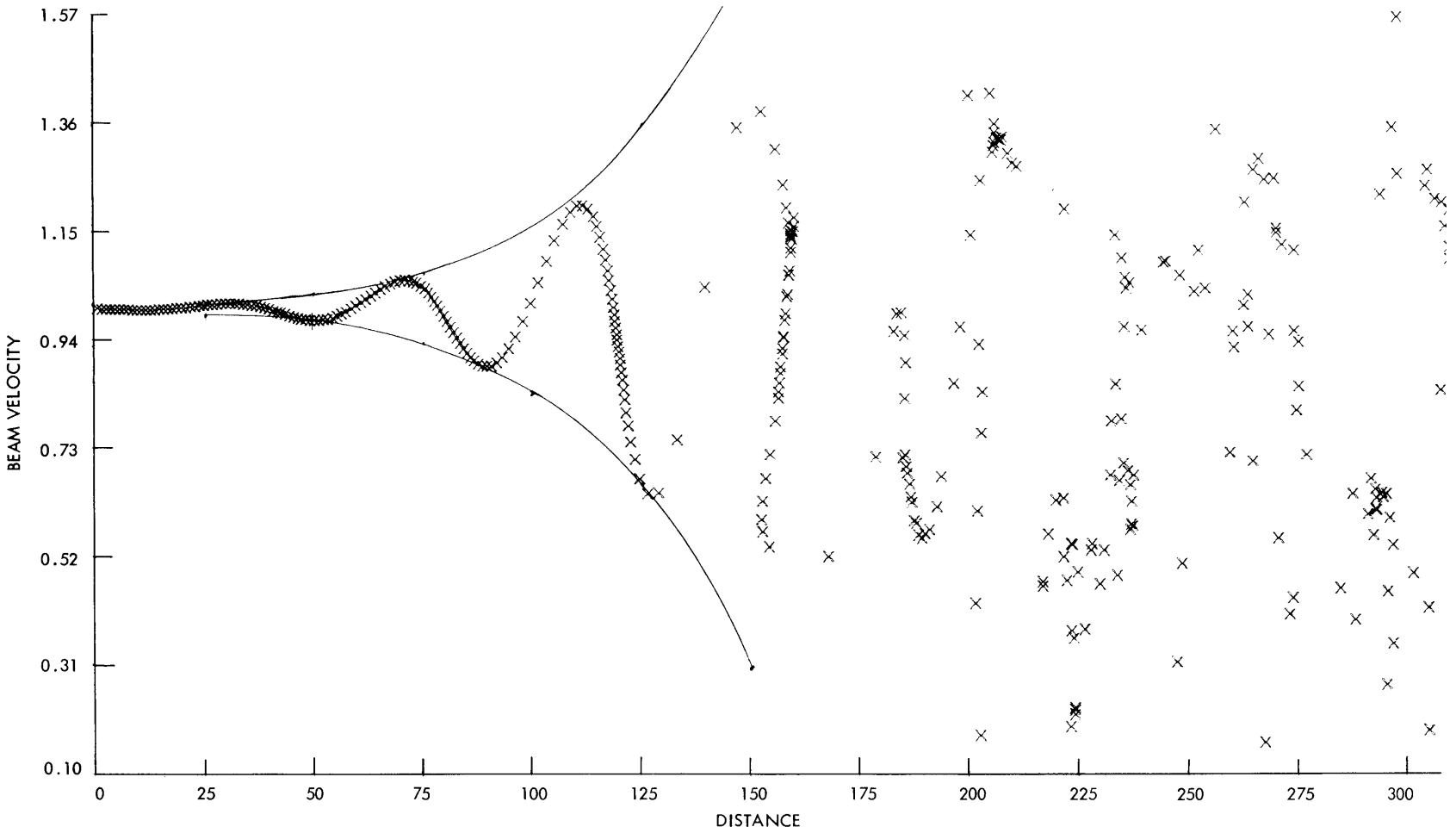


Fig. XXI-3. Instantaneous beam-sheet velocity at $t = 300\ \omega_{po}^{-1}$, where $\omega_{po}^2 = e\rho_o/m\epsilon_o$, $\rho_o(z) = 0.15\ \rho_o + 0.001\ z$. Beam velocity is 0.1 per cent modulated at $\omega = \sqrt{0.15}\ \omega_{po}$.

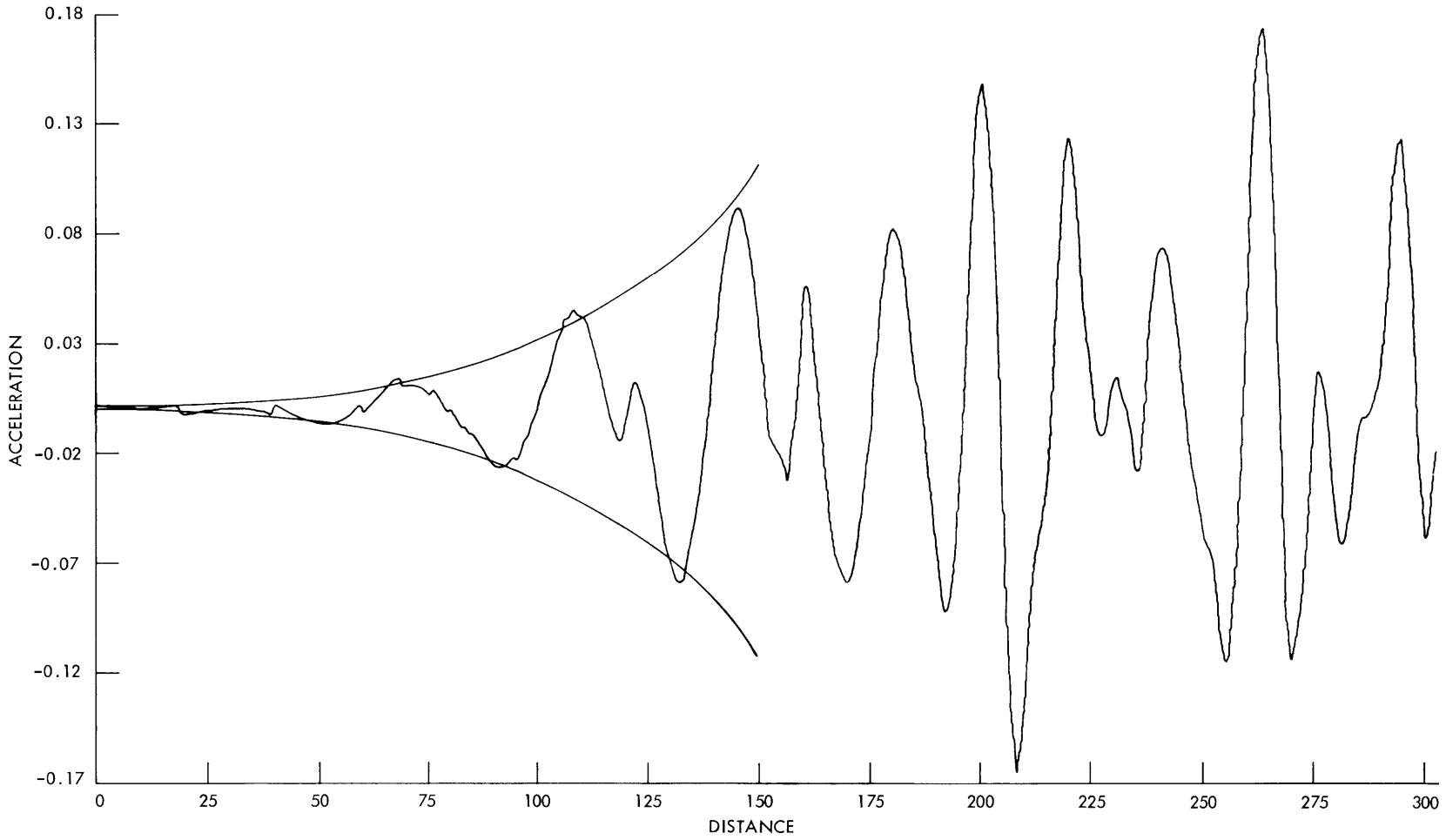


Fig. XXI-4. Instantaneous acceleration of a test particle at z. Times normalized to $\omega_{po}^{-1}$, distances to 0.4 $v_o$ $\omega_{po}^{-1}$.

## 5. SHEET MODEL OF A PLASMA SLAB

We have continued the study of nonlinear plasma slab oscillations with a charge-sheet model.[1,2] The oscillations were initiated by a uniform displacement $\delta$ of an electron cloud that is cold in equilibrium and has thickness d. Several new aspects of the investigation are reported here.

### Dependence of the Scrambling Rate on Initial Perturbation

From electron-sheet trajectories given previously,[2] it can be seen that for small initial displacements the scrambling which originally occurs near the surface propagates in toward the center of the slab at a constant rate. It has been noted that the rate of scrambling propagation is a function of the initial displacement. For the data points shown in Fig. XXI-5, the rate of scrambling propagation is directly proportional to the initial displacement. The rate $R_s$ is described by

$$R_s = 1.33\, f_p \delta, \tag{1}$$

where $f_p$ is the plasma frequency in cycles per second, and $\delta$ is the initial displacement. The numerical factor was determined from Fig. XXI-5. Since the scrambling propagates

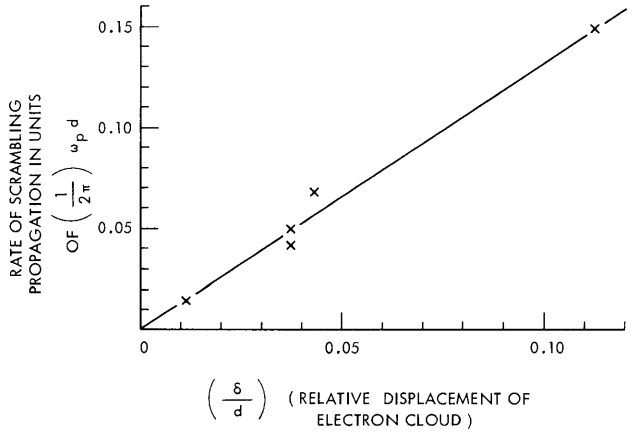


Fig. XXI-5. Rate of scrambling propagation as a function of initial displacement.

in from both sides of the slab, the time, $\Delta t$, at which the ordered plasma oscillations in the entire slab have been destroyed is given by

$$\frac{\Delta t}{T_p} = 0.38\left(\frac{d}{\delta}\right),$$

where $T_p$ is one plasma period, $T_p = 1/f_p$.

## Maximum Energy in the Random Motion

The initial energy given to the slab by a uniform displacement perturbation is entirely in the form of potential energy. If $U_o$ denotes the initial energy per unit area of the slab, we have

$$U_o = \frac{1}{2} m(\omega_p \delta)^2 N\left[1 - \frac{1}{3}\left(\frac{\delta}{d}\right)\right], \tag{2}$$

where N is the total number of particles per unit area, and m is the mass of an electron. The second term inside the brackets is due to the nonuniform electric field near the boundary. Note that for small displacements, $U_o \approx \frac{1}{2} m(\omega_p \delta)^2 N$.

As the scrambling propagates into the slab, the number of particles $N_s$ that have scrambled (those that are no longer oscillating coherently at the plasma frequency) steadily increases. These particles initially had a total energy given by

$$U_s \cong \frac{1}{2} m(\omega_p \delta)^2 N_s. \tag{3}$$

If the scrambled particles are assumed to have a Maxwellian velocity distribution f(V) given by

$$f(V) = \frac{N_s}{\sqrt{2\pi}} \left(\frac{d}{\lambda_D}\right) \frac{1}{\omega_p d} \exp\left[-\frac{1}{2} V^2 \left(\frac{d}{\lambda_D}\right)^2\right], \tag{4}$$

where $V = \frac{v}{\omega_p d}$ and $\lambda_D^2 = \frac{kT}{m\omega_p^2}$, the total kinetic energy of these particles would be

$$U_{Th} = \int_{-\infty}^{+\infty} \frac{1}{2} m\, v^2 f(v)\, dv \tag{5}$$

or

$$U_{Th} = \frac{1}{2} m\, N_s (\omega_p \lambda_D)^2. \tag{6}$$

We can obtain an upper bound to the temperature or Debye length, $\lambda_D$, of the scrambled particles by assuming that all of the initial energy given to the scrambled particles appears as random kinetic energy. Using Eq. 3 and 6, we find

$$\lambda_D \approx \delta. \tag{7}$$

## Numerical Example

The bar-graph velocity distribution for scrambled particles is shown in Fig. XXI-6 for a slab modeled by 129 electron sheets. The distribution was averaged in time over one plasma period when $t/T_p \approx 16$. The initial displacement was $(\delta/d) = 0.0117$, so that

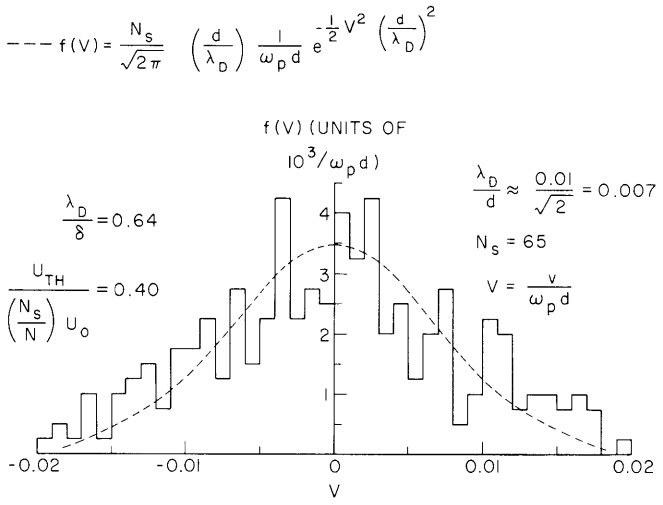


Fig. XXI-6. Time average velocity distribution of scrambled particles for $t/T_p \approx 16$, and $\frac{\delta}{d} = 0.0117$.

at this time (in agreement with Fig. XXI-5) approximately half of the particles have scrambled, or $N_s = 65$. A Maxwellian was fitted to the bar-graph and the Debye length was determined to be

$$\frac{\lambda_D}{d} = 0.007. \tag{8}$$

Thus $\frac{\lambda_D}{\delta} = 0.64$, and we find that approximately 40 per cent of the initial energy given to the scrambled particles appears as energy in the random motion.

H. M. Schneider

## References

1. H. M. Schneider and A Bers, "Dynamics of the Plasma Boundary," Quarterly Progress Report No. 78, Research Laboratory of Electronics, M. I. T., July 15, 1965, pp. 114-119.

2. H. M. Schneider, "Dynamics of the Plasma Boundary," Quarterly Progress Report No. 80, Research Laboratory of Electronics, M. I. T., January 15, 1966, pp. 128-129.

## 6. STABILITY CRITERIA FOR DISPERSION RELATIONS CONTAINING BRANCH POINTS

The stability criteria of Bers and Briggs were developed for plasma dispersion relations, $\Delta(\omega, k)$, which are single-sheeted in the k-plane.[1] The application of the criteria to dispersion relations which have branch cuts has been studied,[2] and some additional thoughts concerning this last type of dispersion relation are presented here.

Many dispersion relations have no branch points with the k-plane and can be analyzed

perfectly well by the original formulation of the stability criteria. It should be pointed out that the expression for the roots, $\omega(k)$, obtained from the dispersion relation $\Delta = 0$, has branch points in the k-plane, and a number of sheets corresponding to the number of roots of $\omega$ for a given k. This does not mean that the dispersion relation has branch points. The original formulation of the stability criteria only breaks down when the dispersion relation itself is associated with more than one sheet in the k-plane.

One example of a dispersion relation with a branch line in the k-plane is the following one for longitudinal plasma waves in a single-species plasma:

$$\Delta(\omega, k) = 1 - \frac{\omega_p^2}{k^2} \int_{-\delta}^{+\delta} \frac{\frac{\partial f_o(u)}{\partial u}}{u - \frac{\omega}{k}}\, du. \qquad (1)$$

$\lim \delta \to \infty$

This function has branch points in the k-plane at $\left(\frac{\mathrm{Re}\ \omega}{\delta}, \frac{\mathrm{Im}\ \omega}{\delta}\right)$ $\left(\frac{-\mathrm{Re}\ \omega}{\delta}, \frac{-\mathrm{Im}\ \omega}{\delta}\right)$. See Fig. XXI-7. This can be demonstrated by taking as $f_o$ a resonance function $f_o = \frac{1}{u^2 + a^2}$. Then $\Delta(\omega, k)$ becomes

$$\Delta(\omega, k) = \frac{1}{\frac{\omega^2}{k^2} + a^2} \left[ \log \left( \frac{\delta - \frac{\omega}{k}}{\delta + \frac{\omega}{k}} \right) - \frac{2\omega}{ak} \tan^{-1} \frac{\ell}{a} \right].$$

It can be seen that this function has branch points as described above.

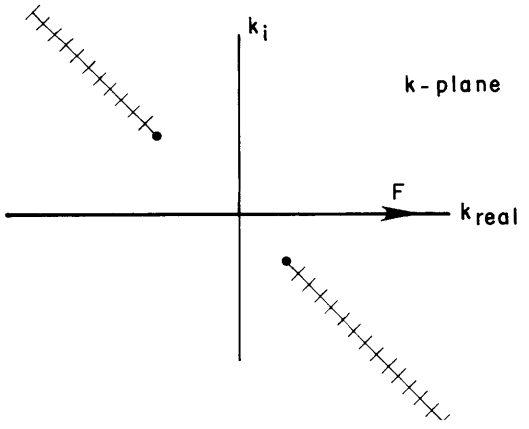


Fig. XXI-7. Branch cut in k-plane for $\Delta(\omega, k)$ describing logitudinal plasma waves, under the assumption of real $\omega$ positive and imaginary $\omega$ negative.

The Fourier contour of the stability criteria is taken along the real k-axis. In applying the stability criteria for single-sheeted dispersion relations, one investigates the roots $k = k(\omega)$ as $\omega$ is swept from the lower half $\omega$-plane to the real $\omega$-axis. Absolute instabilities occur when k-roots pinch the deformed Fourier contour during these sweeps.

It will be shown that this same condition applies to dispersion relations with branch points in the k-plane, Care must be taken however, to make sure that the Fourier contour is really pinched.

The dispersion relation $\Delta(\omega, k)$ in Eq. 1 can be approximated by $\Delta_1(\omega, k)$ and $\Delta_2(\omega, k)$, where

$$\Delta_1(\omega, k) = 1 - \frac{\omega_p^2}{k^2} \int_{-\infty}^{\infty} \frac{\frac{\partial f_o}{\partial u}}{u - \frac{\omega}{k}} du; \qquad \text{Im}\,\frac{\omega}{k} < 0$$

$$\Delta_2(\omega, k) = 1 - \frac{\omega_p^2}{k^2} \int_{-\infty}^{\infty} \frac{\frac{\partial f_o}{\partial u}}{u - \frac{\omega}{k}} du; \qquad \text{Im}\,\frac{\omega}{k} > 0.$$

This approximation is good, except near the origin of the k-plane, around the branch points, and becomes better as $\delta \to \infty$. The regions of validity are shown in Fig. XXI-8, with the Fourier contour on only one sheet.

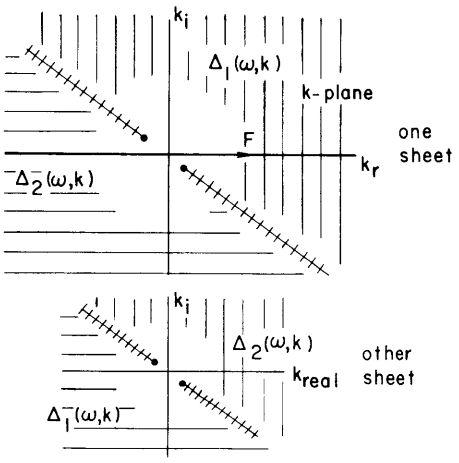


Fig. XXI-8. $\Delta_1$ and $\Delta_2$ approximations to $\Delta(\omega, k)$.

Now consider the roots $k = k(\omega)\big|_{\Delta_1}$ obtained from $\Delta_1$ for sweeps of $\omega$. If they behave as shown in Fig. XXI-9, they most definitely pinch the deformed Fourier contour and predict an absolute instability. If, however, they collide as shown in Fig. XXI-10, more care must be taken to determine whether or not the deformed Fourier contour is really pinched.

In order to see these poles collide, analytic continuation must be performed and the branch lines deformed. In doing this it can be seen the Fourier contour is pushed up and the collision does not pinch the contour. Consequently, no absolute instability is predicted.

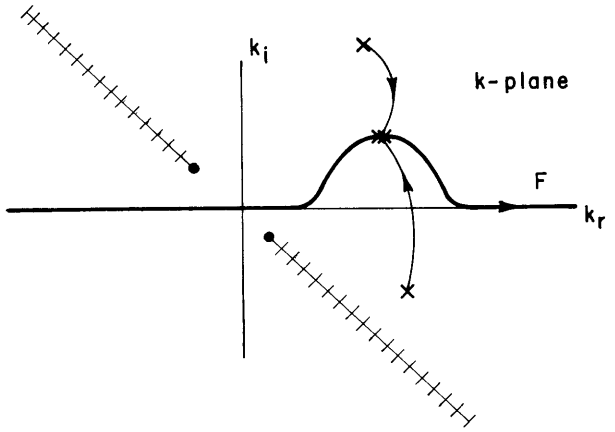


Fig. XXI-9. Absolute instability roots of $\Delta_1(\omega, k)$.

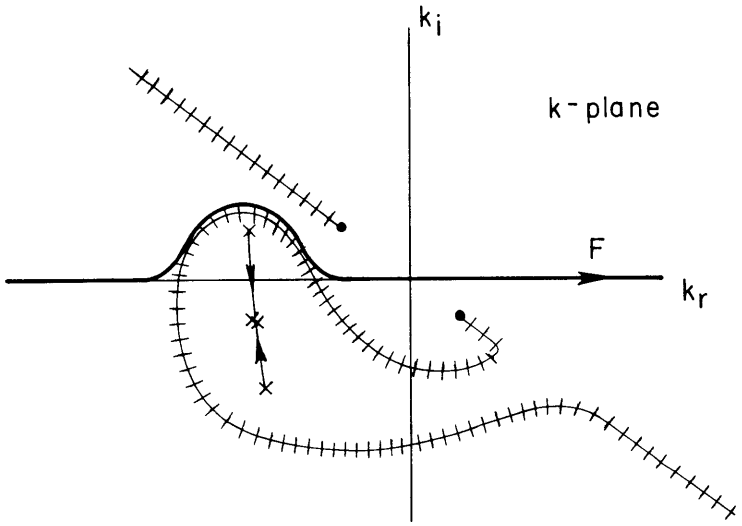


Fig. XXI-10. Roots of $\Delta_1(\omega, k)$ that do not pertain to an absolute instability.

By extending these arguments, it can be seen that a collision of k-roots obtained from $\Delta_1(\omega, k)$ leads to an absolute instability if one root crosses the positive real k-axis, but does not lead to an absolute instability if the collision occurs as a result of a crossing of the negative real k-axis. Similarly, a collision of k-roots obtained from $\Delta_2(\omega, k)$ leads to an absolute instability only if one root crosses the negative real k-axis.

B. R. Kusse

## References

1. R. J. Briggs, Electron-Stream Interaction with Plasmas (The M. I. T. Press, Cambridge, Mass., 1964).

2. B. R. Kusse, "Plasma Dispersion Relations and the Stability Criteria," S. M. Thesis, Department of Electrical Engineering, M. I. T., 1964.

## 7. FINITE LARMOR RADIUS EFFECTS IN THE INTERACTION OF ELECTRONS WITH HIGH-FREQUENCY ACOUSTIC WAVES

We have previously reported[1] on an analysis of the classical dispersion relation for electrons interacting with acoustic waves in a solid.

A physical picture of the interaction and, in particular, the effects of a finite Larmor radius, which come into the electron dielectric constant through the Bessel functions, can be obtained by considering the particle motion along the wave. The energy exchanged between any given particle and the electric field of the wave is given by $\overline{E} \cdot \overline{v}$. As we are considering a longitudinal acoustic wave, $\overline{E}$ is along $\overline{q}$, the wave vector. Thus it is sufficient to consider the zero-order trajectory of a particle along a coordinate axis in the $\overline{q}$ direction as a function of time given by

$$x_q = x_o + (w_{||} \cos\theta)t - \frac{w_\perp \sin\theta}{\omega_c} \cos(\omega_c t + \phi),$$

where $x_o$ and $\phi$ are the arbitrary initial position and phase, $w_{||}$ is the velocity along the external magnetic field, $\overline{B}_o$, $w_\perp$ is the velocity across the magnetic field, $\omega_c$ is the electron-cyclotron frequency, and $\theta$ is the angle between the wave vector and $B_o$. If we consider a longitudinal wave of the form

$$\overline{E} = E_o \frac{\overline{q}}{|q|} \cos(qx - \omega t),$$

then the force on the electron is

$$\overline{F} = -eE_o \frac{\overline{q}}{|q|} \cos\left(qx_o + (q_{||}w_{||} - \omega)t - \frac{q_\perp w_\perp}{\omega_c} \cos(\omega_c t + \phi)\right),$$

where $q_{||} = q\cos\theta$, and $q_\perp = q\sin\theta$. The results of computations on this equation for a particular value of initial position and phase are shown in Fig. XXI-11. Figure XXI-11a is just the electron velocity along $\overline{q}$ attributable to the Larmor orbit; Fig. XXI-11b and 11c are the force on a particle for parameters such that the resonance at $\omega - q_{||}w_{||} + \omega_c = 0$ is satisfied. The first is for a value of $p = \frac{q_\perp w_\perp}{\omega_c}$ (which is $2\pi$ times the ratio of the electron Larmor radius to the wavelength) near the first maximum of $J_1$, and the second for a value of p near the first zero. Figure XXI-11d and 11e are similar, except that here the resonance is $\omega - q_{||}w_{||} + 3\omega_c = 0$ and the p values refer to the first maximum and zero of $J_3$. It is easily seen that the value of $\overline{E} \cdot \overline{v}$ averaged over a cyclotron period is much larger for p values near the maximum of the Bessel functions, and decreases rapidly for values of p near a zero of the Bessel functions.

No conclusions can be drawn about the direction of energy flow between the particles

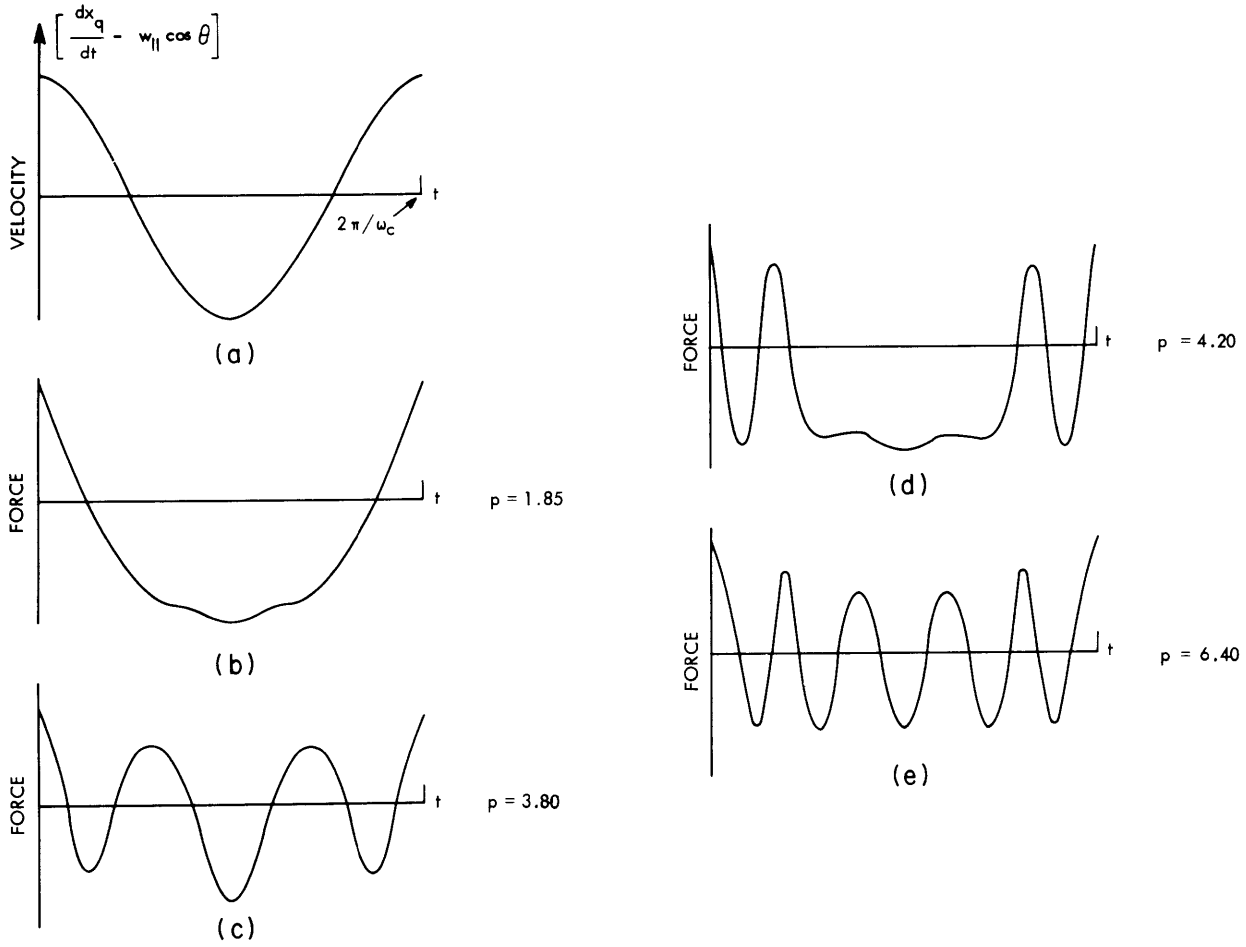


Fig. XXI-11. (a) Unperturbed velocity of a particle along the wave, owing to its Larmor orbit. (b) Force on the particle caused by the wave for parameters such that $\omega - q_{||}w_{||} + \omega_c = 0$ and p is near the first maximum of $J_1$. (c) Same as (b), except that p is near first zero of $J_1$. (d) and (e) Same as (b) and (c), except that the parameters are such that $\omega - q_{||}w_{||} + 3\omega_c = 0$.

and the wave on the basis of this picture. The reason for this is that if the total energy exchange averaged over the randomly distributed initial position and phase is considered, it is easily seen that $\langle \overline{F} \cdot \overline{v} \rangle_{x_o, \phi} = 0$. The direction of energy flow depends, of course, on the derivatives of the distribution function in the manner previously discussed.[1]

S. R. J. Brueck

## References

1. S. R. J. Brueck and A. Bers, Quarterly Progress Report No. 83, Research Laboratory of Electronics, M. I. T., October 15, 1966, pp. 72-76.

# XXI. PLASMAS AND CONTROLLED NUCLEAR FUSION*

## B. Applied Plasma Physics Related to Controlled Nuclear Fusion

### Academic and Research Staff

Prof. D. J. Rose
Prof. T. H. Dupree
Prof. L. M. Lidsky
Prof. E. P. Gyftopoulos
Prof. H. Cheng
Prof. S. Yip
Dr. K. Chung

### Graduate Students

K. R-S. Chen
D. G. Colombant
R. W. Flynn
R. A. Hill
M. Hudis
W. M. Manheimer
G. R. Odette
L. C. Pittenger
A. Sugawara
C. E. Wagner
A. Watanabe

### RESEARCH OBJECTIVES

#### 1. Material and Engineering Experiments Related to Controlled Fusion

We have continued studies of material damage by 14-MeV neutrons, which will be a serious problem in any controlled nuclear fusion reactor. Irradiation of small metal samples continues, with the use of the weak ($10^{10}$ neutrons/sec) Texas Instrument Company accelerator that is available. A radiation damage-detection technique that enables observation of the small expected damage has been used. The measured damage will be compared with theoretical estimates.

We hope to continue experiments on the neutron and gamma-ray spectra from mock-up fusion blanket assemblies.

D. J. Rose, G. R. Odette

#### 2. Feasibility Studies of Controlled Fusion

Calculations of hypothetical controlled fusion system parameters will be carried out to determine the improvement expected by modifying the moderator to contain pure liquid metal, and by modifying other material specifications.

D. J. Rose, L. M. Lidsky

#### 3. Intense Neutron Sources

Preliminary calculations indicate that it may be possible to build a 14-MeV neutron source with $10^{15}$ n/cm$^2$ sec intensity at the target position by using the Mach cone of a freely expanding jet as a windowless gas target. A detailed investigation of such neutron sources has been started with the primary objective of solving the hydrodynamic equations for duct flow with intense heating. This will be followed by an analysis of the system to find the optimal pressure ratios, expansion factors, diffusor design, and so forth.

L. M. Lidsky, D. G. Colombant

*This work was supported by the National Science Foundation (Grant GK-1165).

### 4. Experimental Plasma Turbulence

Work continues on the long "quiescent" plasma column developed during the last two years. To be studied now are (a) ion temperature, including comparison with various theoretical estimates; (b) determination of onset conditions for various unstable modes prevalent in such columns; (c) determination of the conditions for most nearly quiescent operation; (d) propagation of weak (linear) perturbing waves in the quiescent plasma; (e) measurement of the correlation function of the fluctuations in the plasma under various operating conditions; (f) a comparison of conditions in the plasma during "quiescent" operation with predictions of quasi-linear theory.

We have listed more research work than can be accomplished in one year; there are many projects waiting for this popular and useful device.

K. Chung, L. M. Lidsky, D. J. Rose

### 5. Confinement of Hot-Electron Plasmas

We have generated beam-plasma discharge plasmas in mirror, cusp, and stuffed-cusp magnetic fields and are engaged in measurements of their similarities and differences. The mirror-contained plasma is distinguished from the cusp-contained plasma, for example, by a much higher temperature for the energetic group (35 kev vs ~10 kev) and a higher level of density fluctuation. We plan to identify the types of instabilities present in these several systems, giving special attention to distinguishing the instabilities driven by the high- and low-energy electron groups.

L. M. Lidsky, C. E. Wagner

### 6. Particle Diffusion in Weakly Turbulent Plasma

We have studied the motion of particles in weakly turbulent plasma. Particular emphasis has been given to the conditions under which the distribution function satisfies a diffusion equation. Explicit expressions for the diffusion coefficient have been derived. The growth (or damping) rates of the turbulent wave spectrum can be calculated from the rate of energy and momentum transfer between particles and waves.

W. M. Manheimer, T. H. Dupree

### 7. Particle Motion in Large Amplitude Waves

We are attempting to calculate the time evolution of the distribution function for a single nonlinear wave. It is hoped that the solution of this problem can then be applied to strong narrow-band turbulence. In this regime particle trapping, or strong reflections from potential maxima, is an important feature of the motion. This feature is not included in present weak-turbulence theory.

T. S. Brown, T. H. Dupree

### 8. Computer Experiments on Turbulent Plasma

A computer program has been written to compute the particle distribution function for a given arbitrary spectral density of the electric field. The influence of the spectrum on particle motion can be studied in detail and compared with various theories. The distribution function and the electric field are not required to satisfy Maxwell's equation. Dropping this "self-consistency" constraint leads to a much more accurate computer simulation of the Vlasov equation, and also

gives the experimenter complete freedom to specify the spectrum.

R. W. Flynn, T. H. Dupree

## 1. OSCILLATIONS IN THE HOLLOW-CATHODE DISCHARGE ARC

We report here the observation of plasma oscillations in the highly ionized Argon plasma produced by the hollow-cathode discharge arc (HCD).[1] Oscillations were detected by Langmuir probes at various values of plasma parameters. As expected, we observed a close relation between the oscillations and the plasma stability.

In our HCD,[1] we can vary the confining magnetic field in the drift-tube region, the magnetic field over the source region, the neutral pressure in the drift-tube region, the gas-feed rate through the hollow cathode, the gas-feed rate through the hollow anode, the current flow to the anode plate and the column length of the drift tube. Although varying each parameter may affect others, we can vary them rather freely in some restricted regions. In this observation we set the column length at its maximum, and the cathode feed rate at 1 atm-cc/sec, unless it is otherwise noted. We used 1/8" I.D., 0.015" thick, tantalum tube for the cathode, and the inner radius of each baffle was 1 5/8". The probes were located in the drift tube near the baffle and also near the axial mid-point. The radial positions of the probes were changed, and the probes were either floated or biased to the ion saturation voltages. Typically, the plasma density was around $10^{13}$/cc and the radius of the arc column was 1/2".

At fixed gas-feed rate and drift-tube magnetic field, we found significant changes in the frequencies and magnitudes of the oscillations as we varied the source magnetic field. In Fig. XXI-12 we show a series of oscilloscope pictures of power spectra and time-resolved responses of the oscillations. The probes were located 1/4" from the axis and floating. At lower source magnetic fields (a, b or e), there are distinctive signals at 75 kc and its multiples. In fact, we observed similar oscillations at other drift field values. The interesting point is that the fundamental frequency is almost at the ion-cyclotron frequency, which is 75 kc for this particular case. Harmonics are very strong for these oscillations. We also noticed that this oscillation disappears abruptly as we increase the source magnetic field over a certain value. If we compare Fig. XXI-12d and 12e, we see that the disappearance of this oscillation is very sudden, and the plasma column itself undergoes sudden changes in its density and brightness. Note the doubling of the neutral pressure despite the very small change in the source magnetic field. Also, the current to the anode plate changes a lot, although we do not change the gas-feed rate or the external load resistance. Notice in Fig. XXI-12b that when we increased the neutral pressure by an additional anode gas feed, we found that the harmonics were very much subdued, and the oscillation could be relatively reduced somewhat, as compared with the density changes of the plasma.

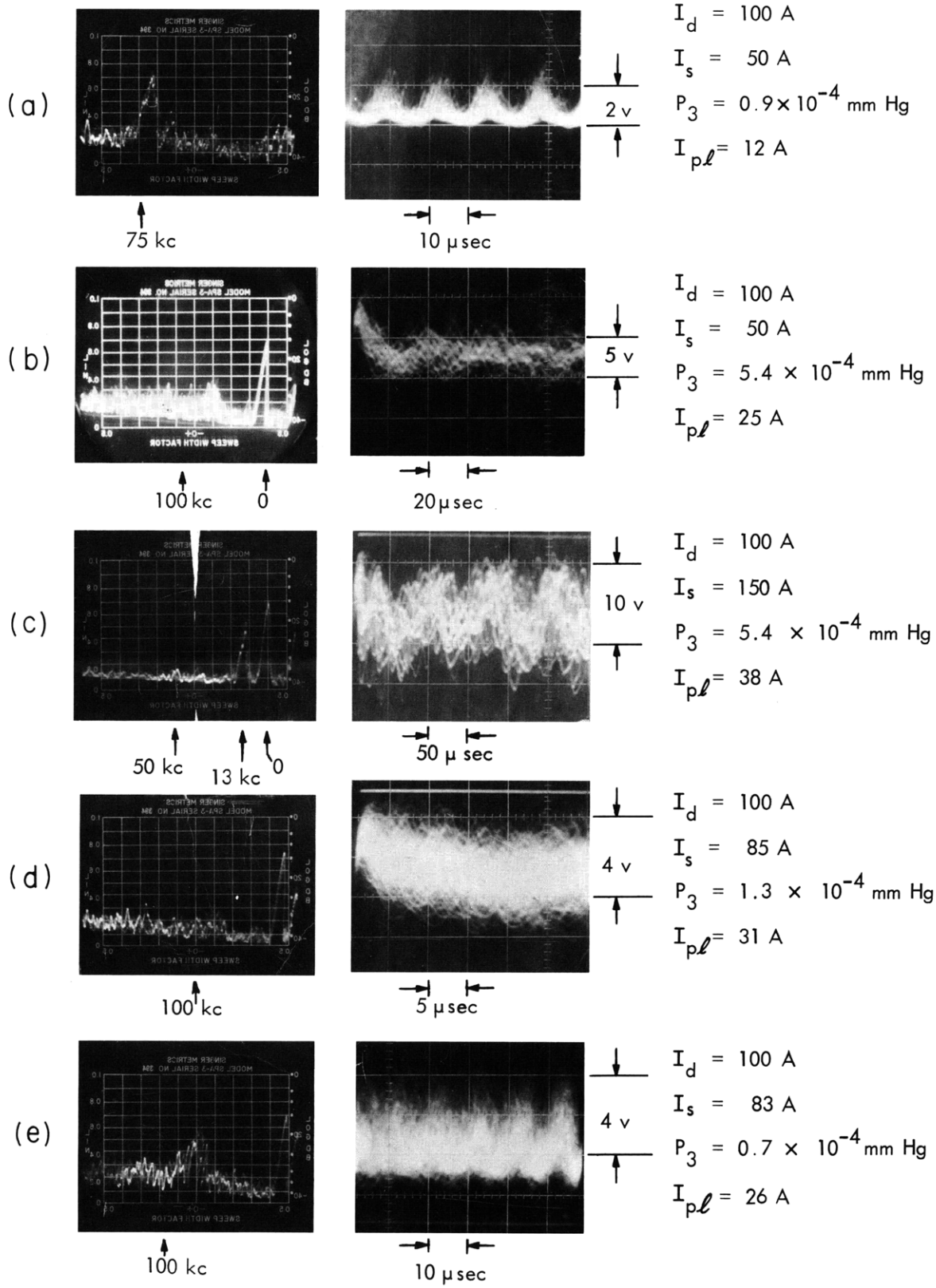


Fig. XXI-12. Power spectra and time-resolved responses of the oscillations.

As we increased the source magnet far beyond the critical value, we found a new kind of oscillation at lower frequencies (Fig. XXI-12c). Contrary to the other kind of oscillations, these new oscillations are very strong at the edge of the plasma, and we could detect a sizable signal far from the axis. In the series of pictures in Fig. XXI-13,

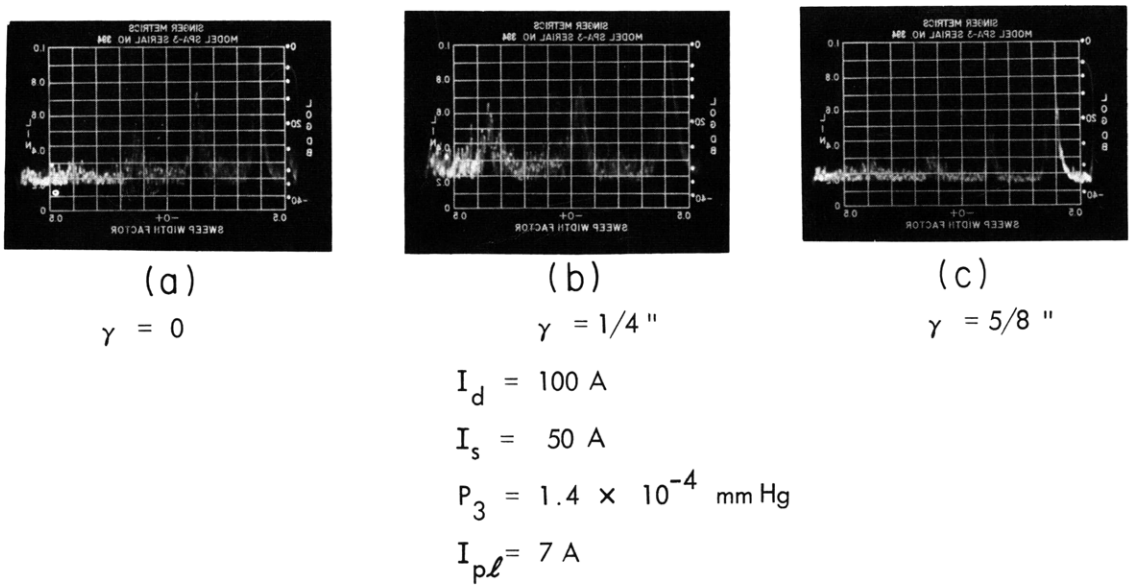

(a) $\gamma = 0$

(b) $\gamma = 1/4"$

(c) $\gamma = 5/8"$

$I_d = 100$ A

$I_s = 50$ A

$P_3 = 1.4 \times 10^{-4}$ mm Hg

$I_{p\ell} = 7$ A

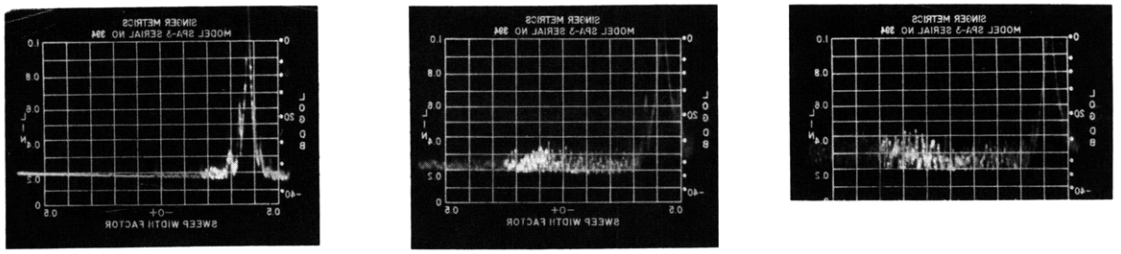

(d) $\gamma = 1"$

(e) $\gamma = 3/8"$

(f) $\gamma = 1/8"$

$I_d = 85$ A

$I_s = 117$ A

$P_3 = 4.3 \times 10^{-4}$ mm Hg

Fig. XXI-13. Radial profile of the oscillations.

we display the signals from different radial positions. We note smaller signals near the center (Fig XXI-13e vs 13f) in the case of lower frequency oscillations. Previously reported "quiet" plasma,[2] which was produced by the same HCD machine, could be

obtained by controlling the magnetic fields to somewhere near the critical values at which the sudden change of plasma density and the onset of plasma oscillation occurred. In order to obtain the "quiet" plasma, we must reduce the low-frequency type of oscillation by lowering the source magnetic field to its critical

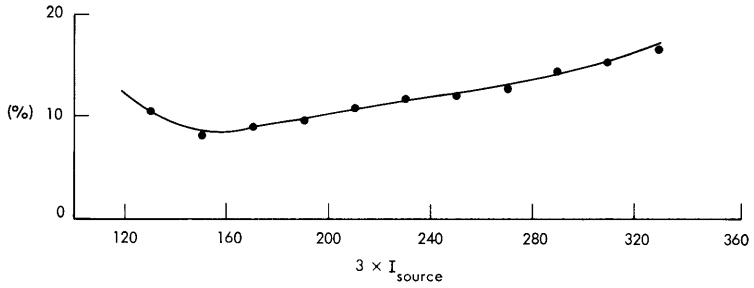


Fig. XXI-14. Percentage of fluctuations with respect to the plasma density.
Cathode Feed ≈ 1 atm-cc/sec
$I_d$ = 125 A $\Longrightarrow$ $B_d \approx 2.5$ kGauss
Anode Feed = 0.1 atm cc/sec
$\gamma = \frac{1}{2}$ in. (near the edge of the plasma).

value and introducing a small amount of the anode gas feed. In Fig. XXI-14 we see the percentage density fluctuation with respect to the source magnetic field. The minimum value of the fluctuation percentage in this particular set of parameters is rather high (8%). If we had measured at the center of the plasma column, we would have recorded a much lower value. This is due to higher plasma densities and lower fluctuation level at the center. Incidentally, the fluctuation illustrated by Fig. XXI-14 was measured by the probes biased at ion-saturation voltages.

The probes biased to ion-saturation voltages registered similar responses with the probes floated. Thus we speculate that the oscillations are electrostatic. Using several probes located at different positions axially and azimuthally, we studied the propagation of the oscillation. We found that the higher frequency oscillations associated with the ion-cyclotron frequency propagate from the anode to the cathode with the phase velocity very close to the ion acoustic wave phase velocity. On the contrary, the lower frequency oscillation, which appeared at higher source magnetic fields, was detected as moving from the source region to the anode. We speculate that this oscillation may be due to the relative motion of layers of the plasma in the baffle region and thus has a hydrodynamic origin. An independent study of the effects of the baffles is under way.

To summarize, we observed two types of plasma oscillations in the Argon plasma produced by the HCD and established the close relation between the plasma oscillations and the plasma stability, which is very helpful in obtaining the "quiet" plasma.

K. Chung

References

1. J. C. Woo, L. M. Lidsky, and D. J. Rose, Quarterly Progress Report No. 76, Research Laboratory of Electronics, M.I.T., January 15, 1965, pp. 130-133.

2. J. C. Woo and D. J. Rose, Quarterly Progress Report No. 82, Research Laboratory of Electronics, M.I.T., July 15, 1966, pp. 163-169.

# XXI. PLASMAS AND CONTROLLED NUCLEAR FUSION

## C. Plasma Magnetohydrodynamic Flows, Waves, and Instabilities

### Academic and Research Staff

Prof. W. P. Allis  Prof. H. A. Haus

### Graduate Students

C. A. McNary  K. R. Edwards

## RESEARCH OBJECTIVES

1. In an MHD plasma, small disturbances of density and temperature are accompanied by small changes in constituent properties, such as conductivity and Hall parameter. An analytic description of all waves that can be supported by a moderate magnetic Reynolds number MHD plasma for all directions of propagation is under study, including the effects of parameter variations on magnetoacoustic and Alfvén wave propagation. A delineation of the MHD environments for which absolute and convective instabilities, if any, can occur is to be found. A study of oscillator and/or amplifier device application feasibility will be undertaken.

H. A. Haus

2. It is well known that glow discharges often exhibit bright spots, and the bright "meniscus" which develops in a hot-cathode discharge has been studied experimentally by Emeleus. Its origin is due to the interaction of the beam of fast electrons from the cathode with the inhomogeneous plasma in this neighborhood. The phenomena of plasma wave amplification and Landau damping are involved. An exact mathematical theory for this and similar phenomena is being developed.

W. P. Allis

## 1. ELECTRON BEAM INTERACTION WITH A SPATIALLY INHOMOGENEOUS TEMPERATE PLASMA

This theoretical analysis of an electron beam-plasma interaction is an attempt to model some of the experimentally observed phenomena that are typical of such a system. Various experimental investigators have observed the randomization of the beam energy and direction, and the abrupt commencement of plasma oscillations at a point a small distance from where the beam enters the plasma.

In the theoretical model now under study, the beam and plasma are considered as separate entities, coupled electrostatically by Poisson's equation. The plasma is assumed to be collisionless and temperate, and the beam is sufficiently diffuse that it does not significantly perturb the plasma as a result of collisions. The geometry of the beam-plasma system consists of a z-directed electron beam having the same

*This work was supported principally by the National Science Foundation (Grant GK-1165).

cross-section dimensions as the plasma. The beam is assumed to be spatially homogeneous and to have a directed velocity, $v_o$, which is a constant. The plasma has a one-dimensional density distribution, $G_k(z)$, and is spacially homogeneous in the other two directions. Under these initial assumptions, the plasma and the beam may be modeled by the collisionless Vlasov equation. This equation is written separately for each species: plasma ions, plasma electrons, and beam electrons. The distribution functions involved are split into zero- and first-order parts, and zero-order parts are assumed to be independent of time and separable in the remaining space and velocity variables. The first-order portions are assumed to be periodic in time; and, because of the comparatively large mass and inertia of the plasma ions, first-order perturbations of the ions are neglected. Substitution of these distribution functions in the Vlasov equation and linearization yields first-order equations for the plasma and beam electrons of the form

$$\frac{\partial \delta f}{\partial t} + \vec{v} \cdot \vec{\nabla} \delta f - \frac{e}{m} \vec{E} \cdot \vec{\nabla}_v \delta f - \frac{e}{m} \delta \vec{E}\, G(z) \cdot \vec{\nabla}_v f = 0. \tag{1}$$

In Eq. 1, $\vec{E}$ and $\delta\vec{E}$ are the zero- and first-order electric fields respectively, $f(\vec{v})G(z)$ is the separable zero-order distribution function, and $\delta f$ is the first-order distribution function. If we assume that the electric fields are z-directed and functions of z only, Eq. 1 may be simplified to

$$\frac{\partial \delta f}{\partial t} + v_z \frac{\partial \delta f}{\partial z} - \frac{e}{m} E(z) \frac{\partial \delta f}{\partial v_z} = \frac{e}{m}\, \delta E(z)\, G_e(z) \frac{\partial f(\vec{v})}{\partial v_z} = 0. \tag{1a}$$

With the following definitions, Eq. 1a may be put into the form

$$\left[\frac{\partial}{\partial v_z} + H\right] \delta f = \frac{\Gamma}{a} \frac{\partial f}{\partial v_z}, \tag{2}$$

where the time dependence is assumed to be of the form $\exp(-j\omega t)$; $eE/m \equiv a$; $\frac{e\delta E(z)\, G(z)}{m} \equiv \Gamma(z)$; H is the operator $\frac{1}{a}(j\omega - v_x D)$; and $D \equiv \frac{\partial}{\partial z}$. Note that only when $a \neq a(z)$, but is a constant, can this formalism be carried out; otherwise commutativity difficulties arise. An additional operator U is so difined that $[\partial/\partial v_z + H]U = 0$, with $U(v_z=0) = 1$ and $UU^{-1} = U^{-1}U = 1$. Straightforward integration then yields

$$U = U(v_z=0) \exp\left[-\frac{1}{a}\left(j\omega v_z - \frac{v_z^2}{2} D\right)\right] = \exp\frac{-1}{a}\left(j\omega v_z - \frac{v_z^2}{2} D\right). \tag{3}$$

Then the particular solution for $\delta f$ may be written in the form

$$\delta f = U \int_0^{v_z} dv_z'\, U^{-1} Q + U \delta f(v_z=0), \tag{4}$$

where

$$Q \equiv \frac{\Gamma(z)}{a} \frac{\partial f}{\partial v_z'} \quad \text{and} \quad U^{-1} \equiv \exp \frac{1}{a}\left(j\omega v_z - \frac{v_z^2}{2} D\right).$$

The formal solution indicated in Eq. 4 may be verified by direct substitution.[1] Although Eq. 4 is only the particular solution of Eq. 1a, it should be noted that the homogeneous solution if of no interest in this analysis. Carrying out the operations indicated in Eq. 4 for a distribution function of the form

$$f_k(\vec{v}) = (\pi v_k)^{-3/2} \exp - \frac{1}{v_k^2}\left[u^2 + (v_z - v_{o,k})^2\right], \tag{5}$$

where $u^2 = v_x^2 + v_y^2$, $v_k$ is the thermal velocity, and $v_{o,k}$ is the directed velocity of the $k^{th}$ specie, yields the following result for $\delta f$:

$$\delta f_k(\vec{v}, v_o) = f_k(\vec{v}, v_o)\left\{1 - \frac{D}{2Aa} + \frac{[j\omega + BD/2A]}{2Aa(v_z + B/2A)}\left[1 + \sum_{n=1}^{\infty} \frac{(-1)^n (2n)!}{n!\left[2\sqrt{A}\,(v_z + B/2A)\right]^{2n}}\right]\right\} \frac{\Gamma}{a}. \tag{6}$$

The infinite series of Eq. 6 results from an asympototic expansion of an error function that arises from the finite limits of integration of the exponential of Eq. 5. Also, $A = 1/v_k^2 + D/2a$, and $B = -\left[j\omega/a + 2v_{o,k}/v_k^2\right]$. Equation 6 is an infinite-order differential equation, and is formally the solution for $\delta f_k$.

Integration of Eq. 6 over velocity space yields a formal result for the first-order particle number density, $\delta n_k$, or the first-order charge density $\delta\rho_k = -e\delta n_k$:

$$\delta\rho_k = -\sum_{n=1}^{\infty} \left[\frac{C_n\left(a + \frac{v_k^2}{2} D\right)^{2n-1}}{\left[\frac{v_k^2}{2}(v_o D - j\omega)^2\right]^n} + \frac{(-1)^n (2n)!}{n!}\left(\frac{2a}{v_k^2}\right)^n \frac{\left(a + \frac{v_k^2}{2} D\right)^{n-1}}{(v_o D - j\omega)^{2n}}\right.$$
$$\left.\cdot\left\{1 + \sum_{m=1}^{\infty} F_{m,n} \frac{\left(a + \frac{v_k^2}{2} D\right)^{2m}}{\left[\frac{v_k^2}{2}(v_o D - j\omega)^2\right]^m}\right\}\right] e\Gamma_k(z), \tag{7}$$

where $C_n = 1 \cdot 3 \cdot 5 \cdot \ldots \cdot (2n-1)$, and

$$F_{m,n} = \frac{[1 \cdot 3 \cdot \ldots \cdot (2m-1)][(2n+1)(2n+2) \cdot \ldots \cdot (2n+2m)]}{(2m)!}.$$

In the case of current interest, two species k are considered, plasma electrons and

beam electrons. By identifying the plasma electrons with the subscript k = e and the beam electrons with k = b; substitution of Eq. 7 in Poisson's equation, with $v_{o,e} = 0$ for the plasma electrons, yields

$$D\delta E = \frac{\Sigma \delta \rho_k}{\epsilon_o} = -\omega_p^2 \sum_{n=1}^{\infty} \left[ \frac{C_n \left(a + \frac{v_e^2}{2} D\right)^{2n-1} (-1)^n}{\left(\omega^2 \frac{v_e^2}{2}\right)^n} + \frac{(2n)!}{n!} \left(\frac{2a}{v_e^2}\right)^n \frac{\left(a + \frac{v_e^2}{2} D\right)^{n-1}}{\omega^{2n}} \right.$$

$$\left. \left\{ 1 + \sum_{m=1}^{\infty} F_{m,n} \frac{\left(a + \frac{v_e^2}{2} D\right)^{2m} (-1)^m}{\left(\frac{v_e^2}{2} \omega^2\right)^m} \right\} \right] g_e(z)\ \delta E(z)$$

$$-\omega_b^2 \sum_{n=1}^{\infty} \left[ \frac{C_n \left(a + \frac{v_b^2}{2} D\right)^{2n-1}}{\left[\frac{v_b^2}{2} (v_o D - j\omega)^2\right]^n} + \frac{(-1)^n (2n)!}{n!} \left(\frac{2a}{v_b^2}\right)^n \frac{\left(a + \frac{v_b^2}{2} D\right)^{n-1}}{(v_o D - j\omega)^{2n}} \right.$$

$$\left. \left\{ 1 + \sum_{m=1}^{\infty} F_{m,n} \frac{\left(a + \frac{v_b^2}{2} D\right)^m}{\left[\frac{v_b^2}{2} (v_o D - j\omega)^2\right]^m} \right\} \right] \delta E(z). \qquad (8)$$

In Eq. 8, $G_e(z) = N_e g_e(z)$, and $G_b(z) = N_b$. Also, $\omega_p^2 = N_e e^2/m_e \epsilon_o$, and $\omega_b^2 = N_b e^2/m_e \epsilon_o$. Equation 8 is the formal differential equation for $\delta E(z)$.

Possible solutions of Eq. 8 have been considered for the case in which a = 0, the zero-order velocity distribution function of the beam is a delta function, $\delta(v_z - v_o)$, and only first-order terms in the plasma temperature, $T_e = \frac{3}{2} v_e^2$, are retained. Then Eq. 8 may be simplidied to

$$D\delta E(z) = -\omega_p^2 \left\{ \left[ \frac{T_e D^3}{\omega^4} - \frac{D}{\omega^2} \right] g_e(z)\ \delta E(z) + \frac{N_b}{N_e} \frac{D}{(v_o D - j\omega)^2} \delta E \right\}. \qquad (8a)$$

For a cold plasma $T_e$ is small and the first term in square bracketts may be neglected. Then, one integration of (8a) yields

$$\left[1 - \frac{\omega_p^2}{\omega^2} g_e(z)\right] D^2\delta E - \frac{2j\omega}{v_o}\left[1 - \frac{\omega_p^2}{\omega^2} g_e(z) + \frac{v_o}{j\omega}\frac{\omega_p^2}{\omega^2} g_e'(z)\right] D\delta E$$

$$+\left[\frac{\left(\omega_b^2 - \omega^2\right)}{v_o^2} - \frac{\omega_p^2}{\omega^2}\left(g_e''(z) - \frac{2j\omega}{v_o} g_e'(z) - \frac{\omega^2}{v_o^2} g_e(z)\right)\right] \delta E = K_1, \tag{8b}$$

where $K_1$ is the integration constant.

For a linear plasma density variation, the coefficient of the second derivative term is of the form

$$1 - a^2(z) = 1 - a_1^2 z,$$

in which it is assumed that

$$a^2(z) = \frac{\omega_p^2}{\omega^2} g_e(z)$$

$$a^2(z) = a_1^2 z$$

$$a^2(z=0) = 0$$

$$a^2(z=1) = a_1^2.$$

Then Eq. 8 may be put in the form of the general Bessel differential equation

$$x^2 D^2\delta E + x[2+2\epsilon x]\, D_x\delta E + \left[\frac{\omega_b^2/v_o^2}{a_1^2} x + 2\epsilon x + \epsilon^2 x^2\right] \delta E = K_1, \tag{9}$$

where $x \equiv \frac{1}{a_1^2} - z$, and $\epsilon = \frac{j\omega}{v_o}$. The homogeneous solution of Eq. 9 is

$$\delta E(x) = x^{-1/2} \exp\left[\frac{-j\omega x}{v_o}\right]\left\{C_1 J_1\left[\frac{2\omega_b}{a_1 v_o} x^{1/2}\right] + C_2 Y_1\left[\frac{2\omega_b}{a_1 v_o} x^{1/2}\right]\right\},$$

or in terms of z,

$$\delta E\left(\frac{1}{a_1^2} - z\right) = \frac{a_1}{\left(1-a_1^2 z\right)^{1/2}} \exp \frac{j\omega}{v_o}\left[z-1/a_1^2\right] \cdot \left\{ C_1 J_1 \left[\frac{2\omega_b}{a_1^2 v_o}\left(1-a_1^2 z\right)^{1/2}\right] \right.$$

$$\left. + C_2 Y_1 \left[\frac{2\omega_b}{a_1^2 v_o}\left(1-a_1^2 z\right)^{1/2}\right]\right\}. \qquad (10)$$

Note that Eq. 10 is singular for $a^2(z) = 1$, the point where the local plasma frequency $\omega_p(z)$ equals the excitation frequency, $\omega$. Figure XXI-15 illustrates the typical wave growth indicated for a plasma density distribution of the form $a_1^2 z$.

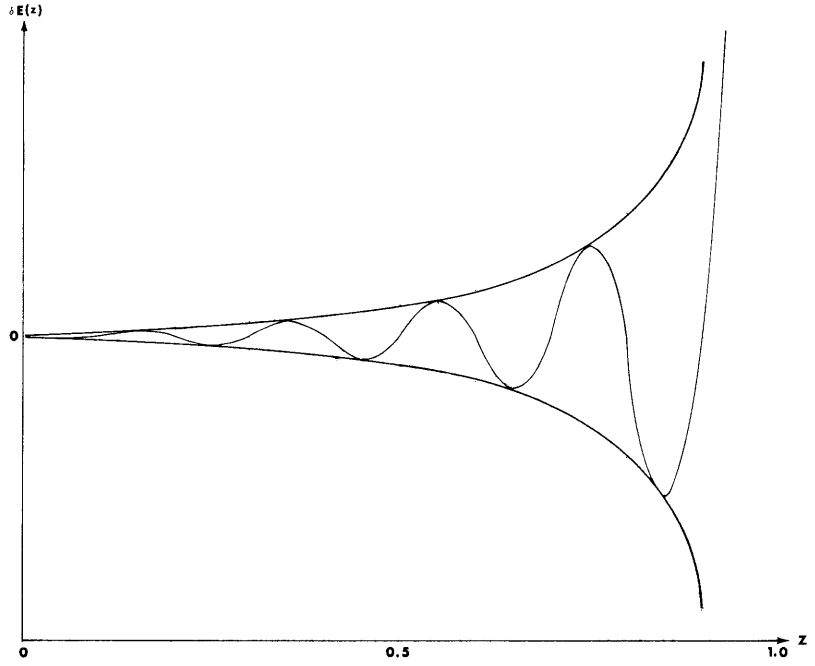


Fig. XXI-15. Typical growth of the first-order electric field; $\omega_b \ll \omega_p$, $a_1^2 = 1$.

The author wishes to acknowledge frequent and invaluable discussions with Professor W. P. Allis which have aided in the development of this analysis to its present state.

C. A. McNary

## References

1. J. C. de Almeida Azevedo, "The Oscillations of an Inhomogeneous Plasma," Ph. D. Thesis, Department of Physics, Massachusetts Institute of Technology, June 1966, pp. 98-101.